energies

MDPI

Article

Effect of Comb-Type Copolymers on the Non-Isothermal Crystallization Behavior of Paraffin in Methyl Ethyl Ketone (MEK)–Toluene Dewaxing

Ying Xiong [1], Xinyao Nie [1,2], Zheng Wang [1], Hongyang Li [1], Yueqin Song [1], Jinan Wang [3], Xiaolong Zhou [1,*] and Lifang Chen [3,*]

[1] School of Chemical Engineering, East China University of Science and Technology, Shanghai 200237, China; y30191174@163.com (Y.X.); xinynie@126.com (X.N.); wz759919498@163.com (Z.W.); lhy182351131902022@163.com (H.L.); songyueqin@ecust.edu.cn (Y.S.)
[2] Liaoning Qingyang Chemical Industry Corporation, Liaoyang 111000, China
[3] ESIQIE, Instituto Politécnico Nacional, Col. Zacatenco, Mexico City 07738, Mexico; jwang@ipn.mx
* Correspondence: xiaolong@ecust.edu.cn (X.Z.); lchen@ipn.mx (L.C.)

Abstract: Two comb-type copolymers were synthesized by modifications of the maleic anhydride-α-octadecene copolymer with aniline (AMAC) and with phenethylamine (EMAC), respectively. The effects of AMAC and EMAC on the non-isothermal crystallization kinetics of the MEK–toluene dewaxing process were comparatively investigated. The results showed that, under the optimum process conditions, the addition of 100 ppm AMAC or EMAC could increase the yield of dewaxed oil (DWO) from 67.21% to 70.87% or 69.90%, respectively, and increase the filtration rate by 80% and 70%, respectively. The non-isothermal crystallization kinetics analysis showed that the crystallization process conformed to Mo's equation, and the addition of AMAC and EMAC slowed down the crystallization rate of paraffin. The polarizing light microscope observations revealed that the addition of AMAC promoted the formation of snow flower-like crystals, and the EMAC addition led to the crystals having longer rods with a relatively complete morphology. This work provided useful experimental data for a better understanding of the roles of comb-type copolymer additives in the MEK–toluene dewaxing process.

Keywords: MEK–toluene dewaxing; comb-type copolymer; paraffin crystal; non-isothermal crystallization

Citation: Xiong, Y.; Nie, X.; Wang, Z.; Li, H.; Song, Y.; Wang, J.; Zhou, X.; Chen, L. Effect of Comb-Type Copolymers on the Non-Isothermal Crystallization Behavior of Paraffin in Methyl Ethyl Ketone (MEK)–Toluene Dewaxing. *Energies* **2022**, *15*, 3989. https://doi.org/10.3390/en15113989

Academic Editors: Mohamed Mahmoud and Zeeshan Tariq

Received: 18 April 2022
Accepted: 19 May 2022
Published: 28 May 2022

1. Introduction

Traditional solvent refining, solvent dewaxing, and supplemental refining are the common routes for the production of type I lubricating base oil. However, because of the energy required to cool and distill a large number of solvents, solvent dewaxing is a high-cost process. Therefore, it is of great significance to improve the efficiency of the solvent dewaxing process.

In the paraffin separation of the methyl ethyl ketone (MEK)–toluene unit, the filtration rate is an important factor affected by the crystal structure and size of the paraffin, and the latter two are mainly influenced by the cooling rate [1]. There is a contradiction between the cooling rate and the filtration rate in actual industry production, because a higher cooling rate led to a decrease in the paraffin crystal size and a possible block of the filter cloth; as a result, the cooling rate is slowed down, and the operation time is increased, which reduces the production efficiency of the MEK–toluene unit. Some studies have shown that the crystallization of paraffin was modified by additional copolymers [2–8], while the contradiction between the cooling rate and the filtration rate is alleviated effectively, and the production efficiency of the MEK–toluene process is improved with the copolymer dewaxing aids. Many patents on dewaxing aids have been issued [9–13], including ethylene-vinyl acetate copolymer, polyacrylate copolymer, combinations of copolymers,

and nanohybrid materials. It is noted that various copolymer dewaxing aids have been applied in the industrial solvent dewaxing process in some refineries in China. The research by Guan et al. showed that 800-ppm polyolefin dewaxing aid could increase the filtration rate by 63% and 4.3% of the yield of the dewaxing oil when furfural refined oil was used as the raw material [14], where the yield of dewaxed oil was obtained by dividing the quality of the dewaxed oil by the quality of the raw material. The study by Ren et al. showed that productivity—that is, the treatment capacity of raw material oil per unit of time—could be improved by 26.6% when the dosage of SM-40 was 3600 ppm [15]. Wang et al. showed that SDA1615 applied to Xinjiang vacuum gas oil (VGO4) and could improve the filtration speed by more than 300% [16]. However, because of the high price and high dosage of dewaxing aids, the cost of solvent dewaxing significantly raised.

Three main roles of dewaxing aids were proposed according to previous investigations: nucleation, adsorption, and eutectic theory. For the nucleation proposal, the dewaxing aid precipitates at a temperature higher than the wax precipitation point of the oil, which transforms into the center of the crystal growth [17,18]. For the adsorption theory, the dewaxing aid is adsorbed around the crystals; then, many crystal molecules can be adsorbed by its long main chain or side branches, making the fine crystals aggregate into large crystal particles and avoid the formation of a three-dimensional network. The eutectic theory proposed that, during the cooling operation, there existed an interaction between the nonpolar carbon chain of the filter aid and the carbon chain of paraffin molecules with similar carbon numbers, leading to the agglomeration of crystals and, then, the formation of larger aggregates [19]. In addition, the growth rate of paraffin crystals is inhibited by dewaxing aids in the horizontal direction, while the growth rate of paraffin crystals in other directions is promoted. Subsequently, the formation of a three-dimensional network structure with poor permeability is prevented. Finally, through one or more of nucleation, adsorption, and eutectic, the dewaxing aids can effectively enhance the filtration rate and improve the productivity of the MEK–toluene process. It is noteworthy that the dewaxing aids may interact with and disperse asphaltene nanoaggregates and then impact the wax crystallization mechanism. Li et al. found that if the large aggerates of asphaltene are dispersed or their precipitation is inhibited, the growth of wax crystals in the crude oil can also be suppressed [20]. The study by Cheng et al. showed that the polymers bearing both aromatic and aliphatic groups can effectively suppress the precipitation of asphaltenes, thereby inhibiting the growth of wax crystals and reducing the size of wax crystals [21]. Due to the different action mechanisms of different dewaxing aids, the types of dewaxing aids have a great impact on the filtration [22–27]. Currently, a deep understanding of the dewaxing aids in the MEK–toluene unit is still lacking.

In this study, to avoid the disadvantages of the high dosage and high cost of traditional dewaxing aids in the MEK–toluene dewaxing process, two comb-type copolymers were synthesized by modifications of the copolymer (maleic anhydride-α-octadecene) with aniline (AMAC) and phenethylamine (EMAC), respectively. The effects of AMAC and EMAC additives in the MEK–toluene dewaxing process were determined. Various factors such as ketone–aromatics ratio, solvent ratio, and dewaxing temperature have been investigated for the process with three-stage dilution and two-stage deoiling. Finally, the non-isothermal crystallization kinetics of paraffin in VGO4 in the absence and presence of dewaxing aids were comparatively investigated by using differential scanning calorimetry (DSC).

2. Experimental Section

2.1. Materials

Maleic anhydride (99%), benzoyl peroxide (99%), and α-octadecene (95%) were purchased from Shanghai Titan Technology Company, Shanghai, China; aniline (99%), phenethylamine (99%), methyl ethyl ketone (99%), o-xylene (99%), and anhydrous methanol (99%) were purchased from Sinopharm Group, Shanghai, China.

VGO4 was obtained from Sinopec Shanghai Gaoqiao Petrochemical Company, Shanghai, China. The properties of VGO4, including density, composition, etc., are shown in

Table 1. The distribution of the carbon numbers of paraffin in VGO4 is shown in Figure 1, which are measured by the pyrolysis of a gas chromatography-mass spectrometer.

Table 1. Properties of VGO4.

Project	VGO4	Standard Test Method
Density/kg·m^{-3}	893.2	ASTM D1298
Saturates Content/%	85.41	SH/T 0509-2010
Aromatic Content/%	7.13	SH/T 0509-2010
Colloid Content/%	2.83	SH/T 0509-2010
Asphalt Content/%	4.63	SH/T 0509-2010
Viscosity index at 100 °C	11.48	ASTM D445-2019
Solidification point/°C	43	ASTM D5773-2010
Wax Content/%	15.9	ASTM D5442-2017

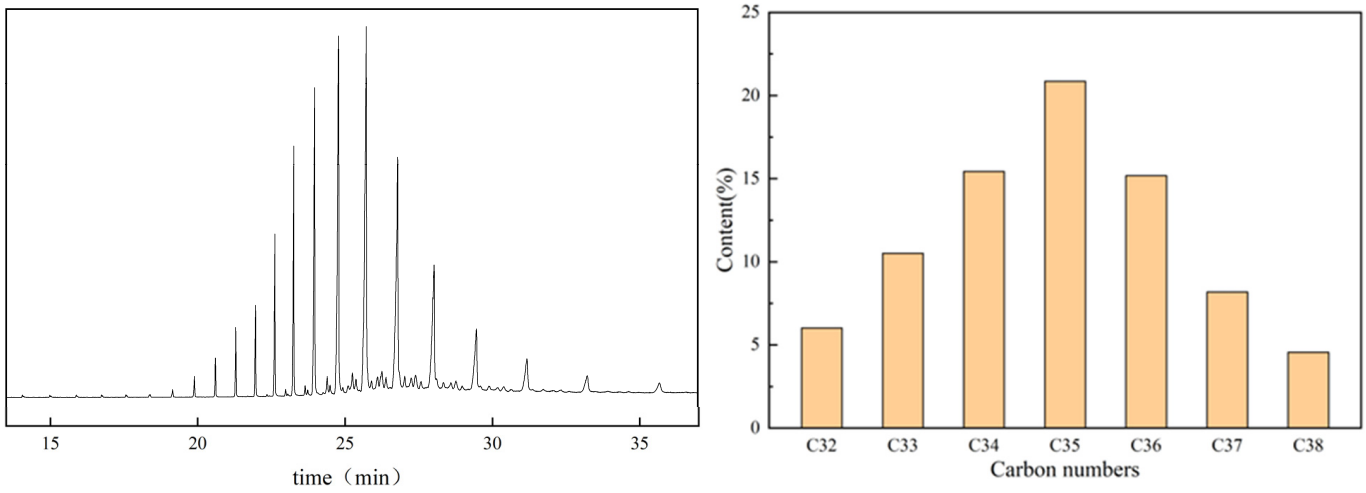

Figure 1. Pyrolysis gas chromatogram and carbon number distribution of paraffin in VGO4.

2.2. Synthesis of AMAC and EMAC

2.2.1. Synthesis of the Maleic Anhydride-α-Octadecene Copolymer

The first step is to prepare maleic anhydride-α-octadecene as the main chain of the comb-type copolymers by free radical polymerization [28]. The reaction equation is shown in Figure 2. The specific operations are as follows. A certain amount of maleic anhydride and α-octadecene were put into a three-necked flask and dissolved in toluene. Then, the initiator benzoyl peroxide (BPO), accounting for 1% of the total mass fraction of the reaction monomer, was dissolved in toluene and loaded into a constant pressure funnel. The constant pressure funnel switch was turned on, and the reaction was performed under the protection of nitrogen for 1 h. After cooling, the product solution was dropped into excess methanol to obtain suspended snowflake-like white particles. Finally, the mixture was filtered and dried to obtain the maleic anhydride-α-octadecene copolymer, which was left for the grafting reaction.

2.2.2. Grafting Reaction

The second step is to obtain comb-type copolymers containing different side chains by grafting the reaction [29]. The reaction equations are shown in Figure 3. The specific operations are as follows. Aniline and α-octadecene maleic anhydride copolymer were put into a three-necked flask at a molar ratio of 1:1, which was dissolved in toluene. The temperature was raised to 75 °C, and the reaction proceeded for 15 h. The product solution was added dropwise to excess methanol, and the final product was obtained by precipitation, washing, filtration, and drying, which was named AMAC. EMAC was

synthesized with phenylethylamine and α-octadecene maleic anhydride copolymer in the same way.

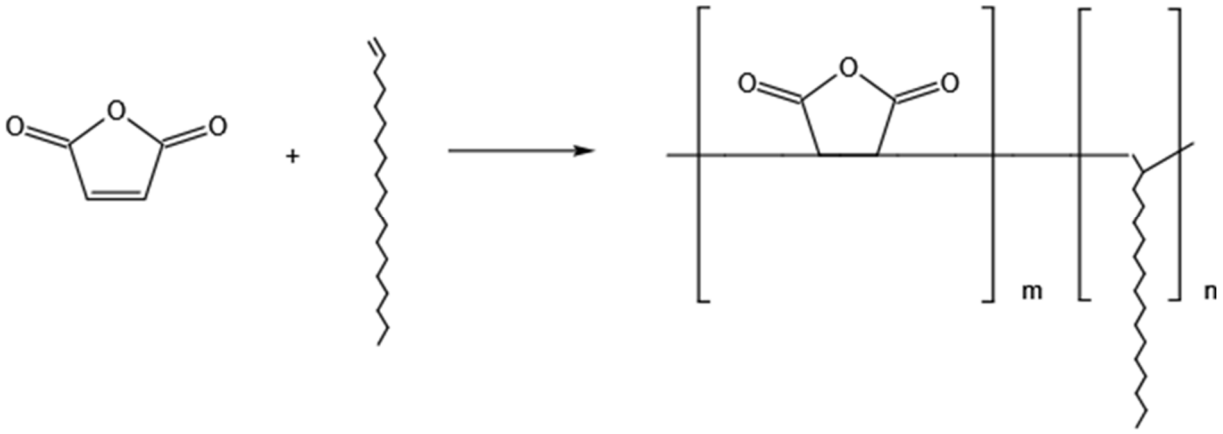

Figure 2. Synthesis of the maleic anhydride-α-octadecene copolymer.

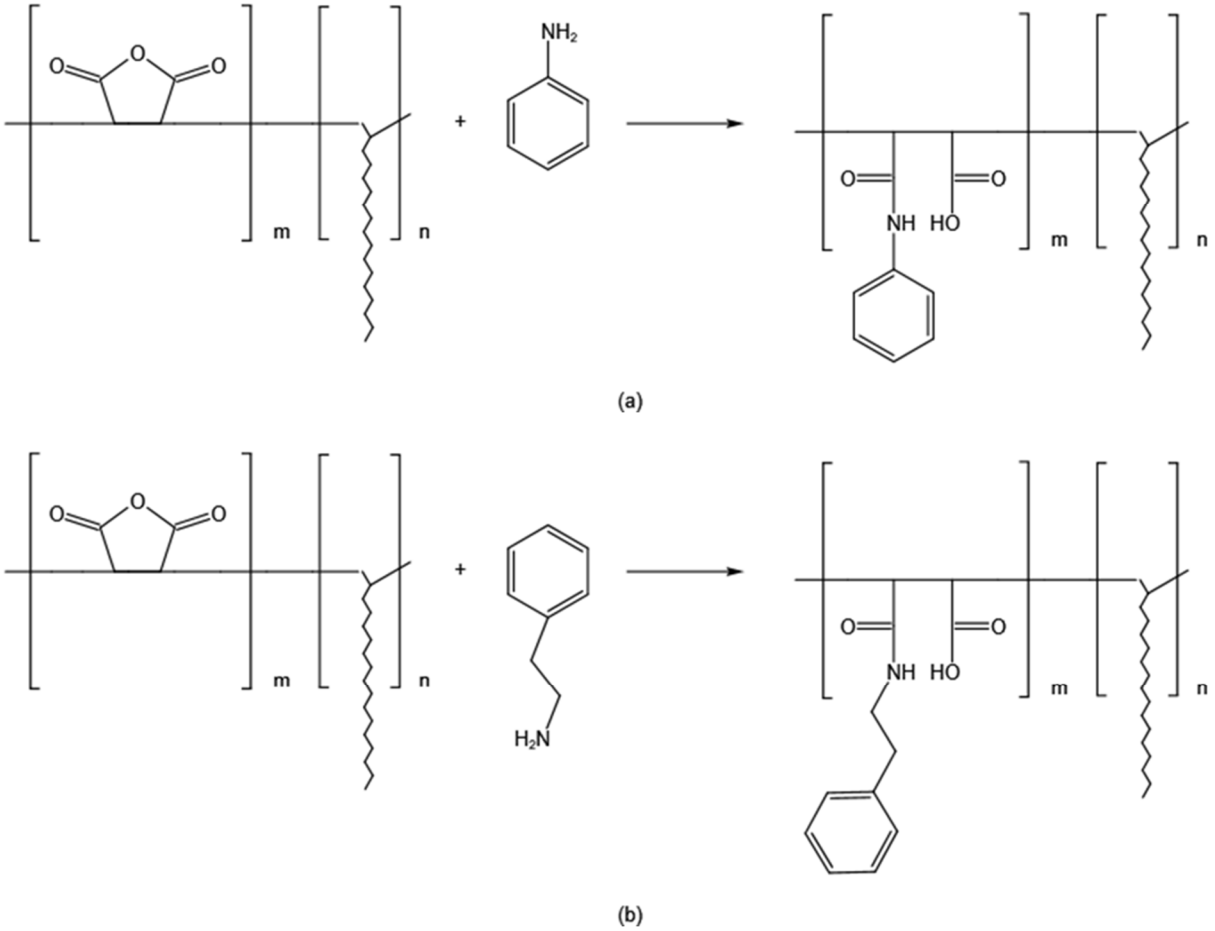

Figure 3. Synthesis of AMAC and EMAC: (**a**) synthesis of AMAC; (**b**) synthesis of EMAC.

2.3. Differential Scanning Calorimetry (DSC)

A DSC8500 differential scanning calorimeter was used for the thermogravimetric analysis. A small amount (5–10 mg) of VGO4 with or without filter aids was weighed in an aluminum pan and sealed. Then, the samples were heated to 80 °C at a rate of 10 °C/min under the protection of nitrogen to ensure that the final temperature was above the melting temperature of the samples. Furthermore, the samples remained at 80 °C for 10 min and

then cooled to −20 °C for scanning at rates of 2.5, 5, 10, and 15 °C/min, respectively. Finally, the non-isothermal crystallization DSC curves of the samples were obtained.

2.4. Polarizing Light Microscope

The crystalline morphology of paraffin in VGO4 was observed through a LEIKADM 2500 with a Linkam THMS 600 cold/hot stage. Firstly, the prepared samples were heated and dissolved into solutions; then, they were dropped onto a glass slide by capillary suction, where they cooled to room temperature. Afterward, the glass slides were transferred to the cold stage, where the temperature dropped to −20 °C at a rate of 10 °C/min, and subsequently, a crystal morphology of the paraffin in VGO4 at −20 °C was observed. Since the crystal shapes of VGO4 were mainly needle-like, the size of the VGO4 crystals was represented properly by the length of VGO4.

2.5. MEK–Toluene Dewaxing

The MEK–toluene dewaxing process consisted of three-stage dilution and two-stage deoiling, as shown in Figure 4. VGO4 was dewaxed, filtered, and distilled to obtain dewaxed oil (DWO) and crude wax; then, the crude wax was deoiled, filtered, and distilled to obtain the deoiled wax (WAX) and foots oil (FO). Various factors such as the ketone–aromatics ratio, solvent ratio, and filtration temperature were investigated. The effect of AMAC and EMAC on MEK–toluene dewaxing was reflected by the yield of DWO, the yield of FO, the yield of WAX, and the relative filtration rate.

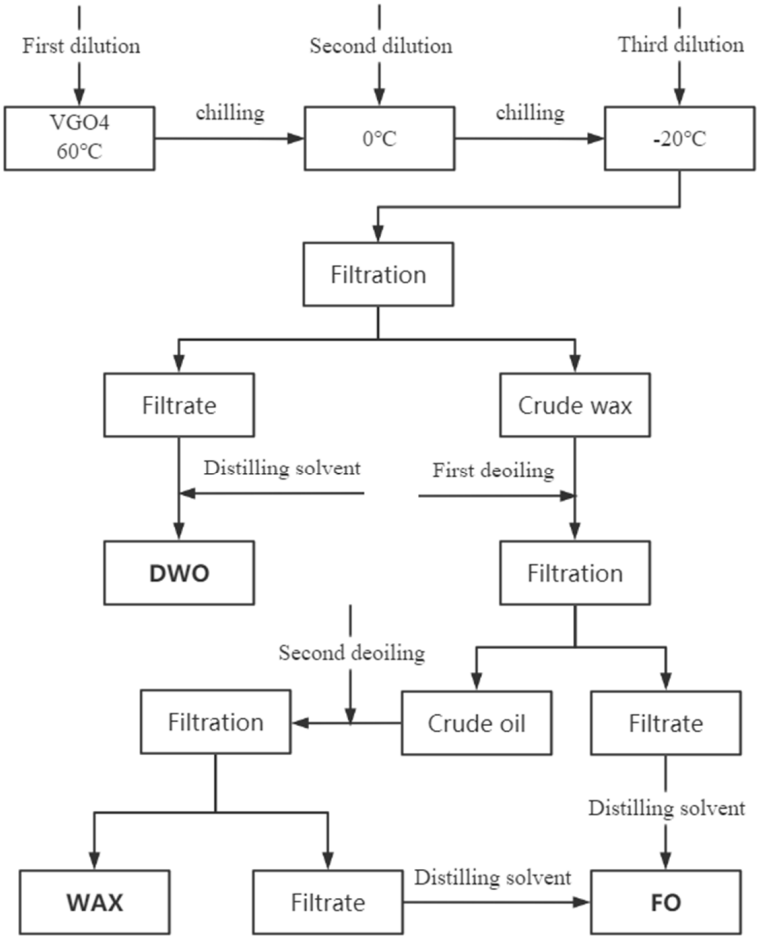

Figure 4. A diagram of the MEK–toluene dewaxing process.

The quality of DWO was expressed by its solidification point, which was measured according to ASTM D5773-2007.

The quality of WAX was expressed by the oil content of WAX, which was measured according to ASTM D721-2017.

3. Results and Discussion

3.1. Synthesis of AMAC and EMAC

The chemical structure and ^{1}HNMR spectra of AMAC and EMAC are shown in Figure 5. Peaks a, b, c, d, e, and f represent the hydrogen of -CH3- in octadecene, hydrogen of -CH2- in octadecene, hydrogen of -CH2- on the backbone of the octadecene, hydrogen of -CH- in octadecene, hydrogen of -CH- in maleic anhydride, and hydrogen of the benzene ring, respectively. These peaks mean that AMAC and EMAC were successfully synthesized. In AMAC, the ratio of hydrogen of -CH3- in octadecene and hydrogen of the benzene ring is 0.59, and in EMAC, the ratio of -CH3- in octadecene and hydrogen of the benzene ring is 0.72, which are calculated from the ratio of the peak areas of a and f obtained by integration of the peaks on the ^{1}HNMR spectra.

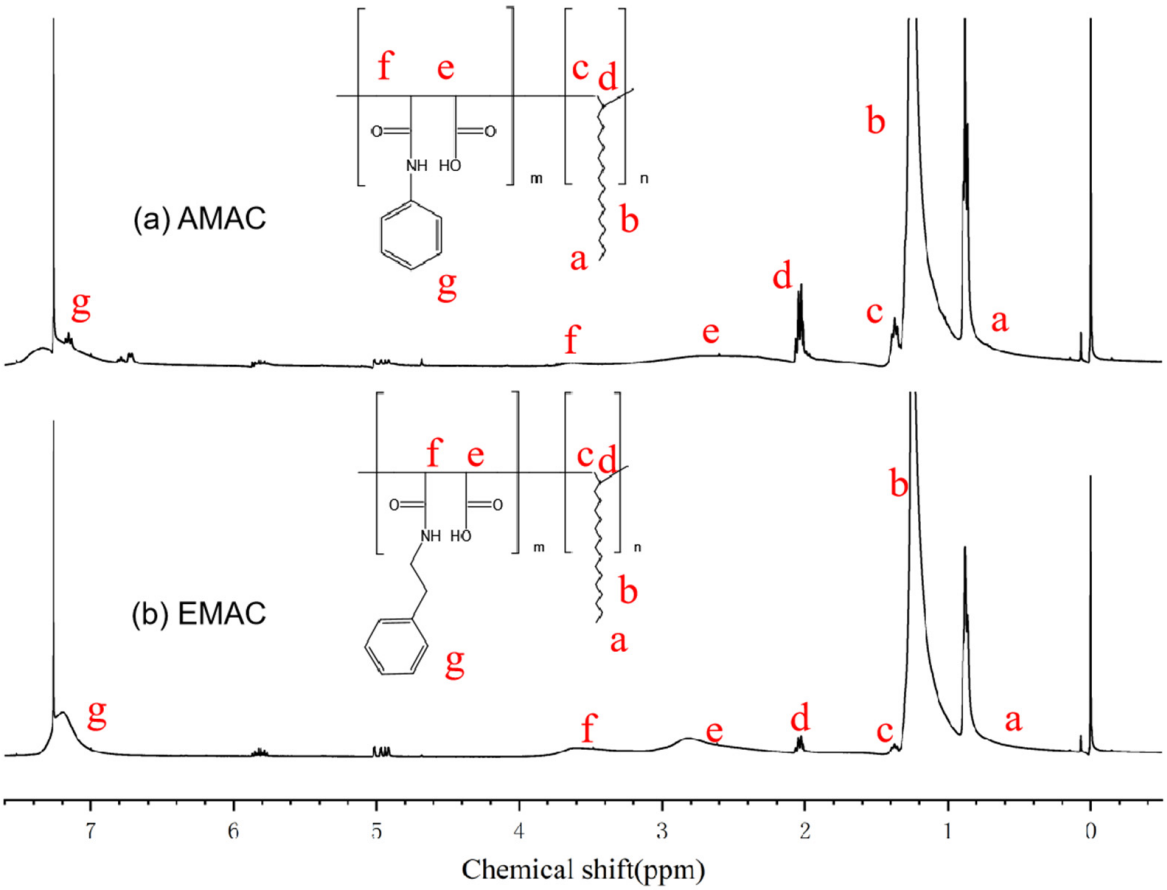

Figure 5. ^{1}HNMR spectra of AMAC and EMAC.

3.2. Process Conditions of Dewaxing Section

3.2.1. Ketone–Aromatics Ratio

The mixture of MEK and toluene was used as the dewaxing solvent. The ketone–aromatics ratio is the ratio of MEK to toluene in the mixed solvent. As a settling agent for paraffin, MEK has a particularly low solubility for paraffin. Meanwhile, although a small amount of paraffin can be dissolved in toluene, oil is easier to dissolve in toluene, because it is highly miscible. Therefore, the optimal ketone–aromatics ratio should be determined first when VGO4 is used as the MEK–toluene dewaxing raw material.

The experimental results of the MEK–toluene dewaxing of VGO4 with different ketone–aromatics ratios are shown in Table 2. It can be found that the yield of DWO and the

solidification point of DWO were inversely proportional to the ketone–aromatics ratio; the oil dissolving ability of the mixed solvent was decreased when the ketone–aromatics ratio was above 60, and the oil was not able to be dissolved completely, resulting in a decrease in the yield of DWO. Simultaneously, the ketone–aromatics ratio below 60 was adverse for the filtration rate, since fine crystal particles were produced in the crystallization of paraffin in toluene. Therefore, in this study, the ketone–aromatics ratio was selected as 60. Higher yields of DWO, WAX, and the oil content of WAX were obtained at this ratio. Additionally, the relative filtration rate reached was the best.

Table 2. Effect of the ketone–aromatics ratio on the MEK–toluene dewaxing of VGO4.

Ketone–Aromatics Ratio		55	60	65	70
DWO	Yield/%	68.36	67.21	66.95	65.49
	Solidification point/°C	−11	−12	−12	−11
WAX	Yield/%	15.17	15.90	15.41	15.60
	Oil content/%	8.92	6.32	7.63	8.69
FO	Yield/%	16.47	16.89	17.64	18.91
Relative filtration rate		0.9	1	0.8	0.7

The filtration rate under the optimum process conditions was set as 1.

3.2.2. Solvent Ratio

The solvent ratio is the ratio of the solvent to the raw material. Generally, the solvent contains light materials less than heavy materials, and the wax content is proportional to the solvent ratio. Therefore, when using VGO4 as the MEK–toluene dewaxing raw material, the optimal solvent ratio should be determined according to its composition and wax content.

The experimental results of the MEK–toluene dewaxing of VGO4 with different solvent ratios are shown in Table 3. As the solvent ratio of the dewaxing section was raised from 3:1 to 5:1, an increase in the relative filtration rate was observed, while the oil content of WAX and the solidification point of DWO were decreased. This can be explained by the decline of the viscosity of the oil at a higher solvent ratio. However, when the solvent ratio was further increased, the trend of the relative filtration rate remained unchanged, but the yield of DWO, the oil content of WAX, and the solidification point of DWO were increased slightly. This is because a small part of the crystallized paraffin was dissolved when the solvent capacity was enhanced due to the high amount of solvent, leading to an increase in the yield of DWO and the solidification point of DWO. Therefore, the solvent ratio of the dewaxing section of the MEK–toluene dewaxing of VGO4 was set as 5:1.

Table 3. Effect of the solvent ratio on the MEK–toluene dewaxing of VGO4.

Solvent Ratio		3:1	4:1	5:1	6:1
DWO	Yield/%	65.60	66.24	67.21	67.74
	Solidification point/°C	−10	−11	−12	−11
WAX	Yield/%	15.39	15.66	15.90	15.35
	Oil content/%	7.22	6.86	6.32	8.01
FO	Yield/%	19.01	18.10	16.89	16.91
Relative filtration rate		0.6	0.8	1	1.1

3.2.3. Dewaxing Temperature

Dewaxing temperature refers to the temperature at which DWO and the crude wax are filtered and separated in the dewaxing section. Since MEK–toluene dewaxing is a physical process, the dewaxing temperature has a significant effect on it. The experimental results

of the MEK–toluene of VGO4 with different dewaxing temperatures are shown in Table 4. Comparing the data in Tables 2–4, relatively speaking, the filtration rate was most strongly affected by the filtration temperature, followed by the solvent ratio. The variation of the ketone–aromatics ratio showed a less important effect on the filtration rate. Maintaining the solidification point of DWO at an acceptable level by increasing the dewaxing temperature is an effective method to increase the filtration rate. According to the results in Table 4, when the dewaxing temperature was higher than −12 °C, i.e., −6 °C, the yield of DWO, the solidification point of DWO, and the relative filtration rate were increased. This was due to the fact that, at dewaxing temperatures higher than −12 °C, part of the crystallized paraffin redissolved. At this time, although the filtration speed was fast, the solidification point of DWO and the oil content of WAX became higher. When the dewaxing temperature was lower than −12 °C, i.e., −15 °C, it was not conducive to the filtration and separation of the oil and paraffin. Therefore, in the present work, the suitable dewaxing temperature of VGO4 was set at −12 °C.

Table 4. Effect of the dewaxing temperature on the MEK–toluene dewaxing of VGO4.

Dewaxing Temperature/°C		−6	−9	−12	−15
DWO	Yield/%	69.27	68.43	67.21	65.82
	Solidification point/°C	−7	−9	−12	−13
WAX	Yield/%	14.37	15.18	15.90	16.07
	Oil content/%	8.18	7.27	6.32	5.93
FO	Yield/%	16.36	16.39	16.89	18.11
Relative filtration rate		1.3	1.2	1	0.7

The experimental process conditions of the MEK–toluene dewaxing of VGO4 were determined by investigating the above single-experimental factors. A process with three-stage dilution and two-stage deoiling was selected, and the solvent ratio of each solvent dilution, dilution temperature, total solvent ratio, filtration temperature, funnel aperture, and filtration pressure difference are reported in Table 5.

Table 5. Experimental process conditions of the MEK–toluene dewaxing of VGO4.

Dewaxing Section		Deoiling Section	
First dilution solvent ratio(V/W)	1.5:1	First deoiling solvent ratio(V/W)	1:1
First dilution temperature/°C	60	First deoiling temperature/°C	0
Second dilution solvent ratio(V/W)	2.5:1	Second deoiling solvent ratio(V/W)	1:1
Second dilution temperature/°C	0	Second deoiling temperature/°C	10
Third dilution solvent ratio(V/W)	1:1	Total solvent ratio(V/W)	2:1
Third dilution temperature/°C	−20	Filtration temperature/°C	10
Total solvent ratio(V/W)	5:1		
Filtration temperature/°C	−12		
Filter area/m^2	0.00145		
Filter pore size/μm	<1.5		
Filter pressure difference/MPa	0.1		

3.3. Investigation on the Dosages of Dewaxing Aids

Although the optimal conditions for the MEK–toluene dewaxing experiment of VGO4 were determined, the yield of DWO, the yield of WAX, and the oil content of WAX were not yet satisfactory. Therefore, a dewaxing aid, EMAC or AMAC, was added to VGO4 during this process before adding the solvent. The changes in the experimental results after adding dewaxing aids are shown in Tables 6 and 7. It could be seen that different dosages of EMAC and AMAC had a more significant effect on the MEK–toluene dewaxing of VGO4. As shown in Table 6, when different dosages of AMAC were added, it was found that the highest yield of DWO, the highest relative filtration rate, and the lowest oil content

of WAX were obtained by using 100 ppm AMAC. Hence, the optimal dosage of AMAC was 100 ppm. The addition of 100 ppm AMAC could increase the yield of DWO by more than 3% and the filtration rate by 80%. Similarly, the optimal dosage of EMAC was 100 ppm. The addition of 100 ppm EMAC could increase the yield of DWO by 2.7% and the filtration rate by 70% (Table 7). In addition, when the dosage exceeded 100 ppm, the relative filtration rate and the yield of DWO were inversely proportional to the dosage. This was because, when the dosage was less than 100 ppm, the existence of comb-type copolymers could form a small number of crystal nuclei at the initial crystallization stage, which attracted paraffin molecules to aggregate each other; when the dosage was more than 100 ppm, the number of crystal nuclei increased at the early crystallization stage, dispersing the accumulation of paraffin and, thus, reducing the size of paraffin, which reduced the size of the paraffin crystals and negatively affected the filtration aid role. Notably, the addition of AMAC could improve the yield of WAX, while, when EMAC was added, the yield of WAX was not improved, but it could reduce the oil content in WAX, which may be related to the different mechanisms of the two dewaxing aids.

Table 6. MEK–toluene dewaxing with different dosages of AMAC.

Dosage/ppm		**0**	**50**	**100**	**150**	**200**
DWO	Yield/%	67.21	68.80	70.87	69.37	68.62
	Solidification point/°C	−12	−18	−24	−22	−21
WAX	Yield/%	15.90	16.14	16.51	16.38	16.25
	Oil content/%	6.32	4.92	4.12	4.38	4.53
FO	Yield/%	16.89	15.06	12.62	14.25	15.13
Relative filtration rate		1	1.4	1.8	1.6	1.4

Table 7. MEK–toluene dewaxing with different dosages of EMAC.

Dosage/ppm		**0**	**50**	**100**	**150**	**200**
DWO	Yield/%	67.21	68.58	69.90	69.11	68.30
	Solidification point/°C	−12	−17	−22	−21	−20
WAX	Yield/%	15.90	15.79	15.66	15.71	15.74
	Oil content/%	6.32	4.12	2.78	3.52	3.78
FO	Yield/%	16.89	15.63	14.44	15.18	15.96
Relative filtration rate		1	1.3	1.7	1.5	1.4

3.4. Polarizing Light Microscope (PLM)

The polarized light microscope photos of the paraffin crystals of three samples at −20 °C (cooling rate is 10 °C/min) are shown in Figure 6. For the VGO4 sample, Figure 6a, most of the paraffin crystals were short rod-like crystals, and they were not tightly contacting each other, with blurred outlines. These observations are probably due to the fact that most of the carbon numbers of paraffin in VGO4 were greater than C_{30} (Figure 1). During filtration, the crystals were small and packed inside the pores and blocked the filter cloth, resulting in the permeability of the wax cake being poor. In addition, although it was difficult for the fine rod-like crystals to form a three-dimensional grid structure of oil-in-paraffin, their larger specific surface area enabled the crystal surface to absorb more oil, leading to an increase in the oil content of WAX and the deterioration of the WAX quality.

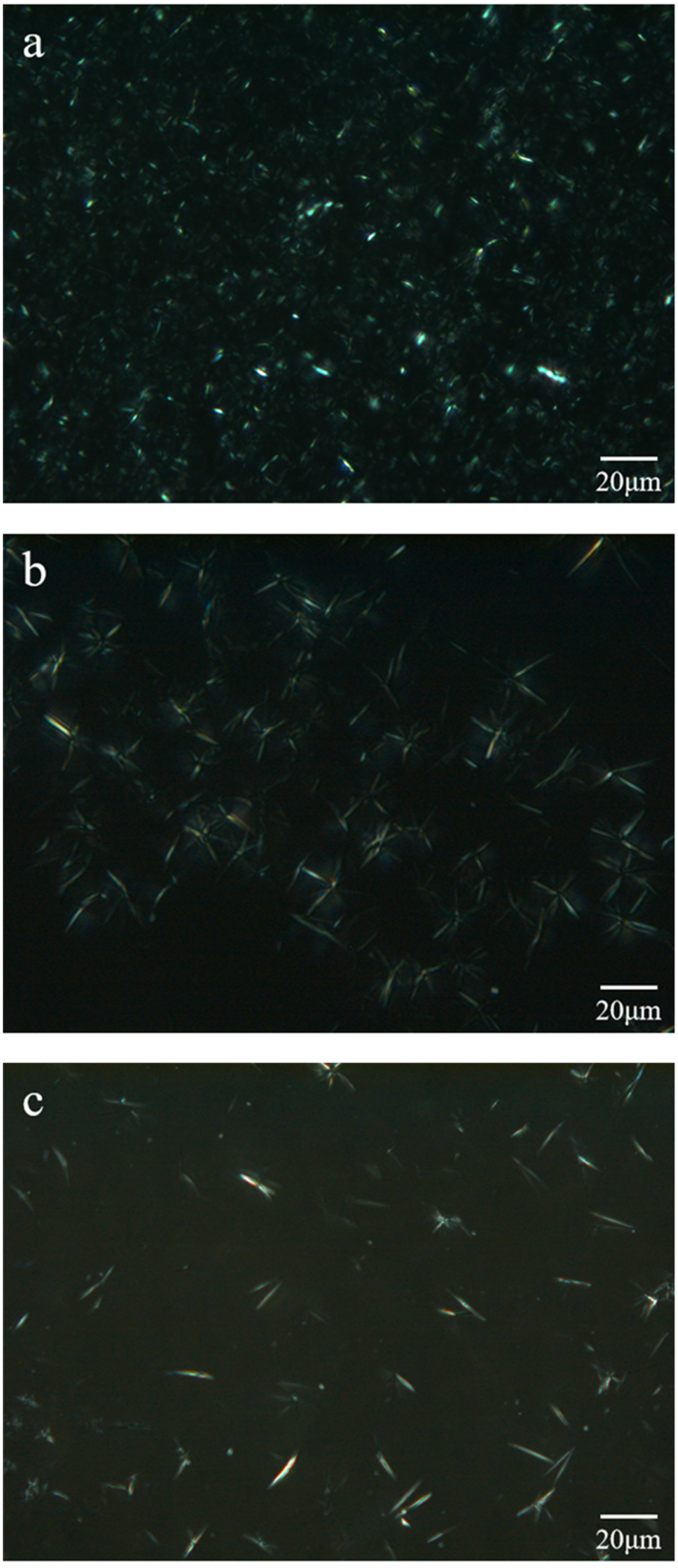

Figure 6. Paraffin crystal micrograph: (**a**) VGO4, (**b**) VGO4 + 100 ppm AMAC, and (**c**) VGO4 + 100 ppm EMAC.

Figure 6b shows that the aggregation of the sample crystals was significantly improved after the addition of a 100 ppm AMAC additive, and the crystals were larger, and they regularly connected to each other to form many three-dimensional crystals with snow flower-like shapes.

Figure 6c shows the crystal morphological features of the sample obtained after the addition of 100 ppm EMAC. The crystallite size was large, with a big diameter. Most of the crystal length was approximately 10 μm. In comparison with the blank VGO4, both AMAC and EMAC additives could effectively increase the size of the paraffin crystals in VGO4 and altered the crystal shapes and morphology. Unlike EMAC, AMAC could also improve the aggregation of the crystals by forming three-dimensional nanocrystals. The different morphologies resulted from the different mechanisms of AMAC and EMAC, which was consistent with the previous experimental results.

3.5. Differential Scanning Calorimetry

The shape and size of the paraffin crystals of VGO4 are affected by its crystallization process and determine their filtration rate. Since the actual MEK–toluene dewaxing is a non-isothermal crystallization process, the study of the paraffin crystallization process is therefore of great significance for improving the production efficiency of the MEK–toluene unit. In this study, the DSC cooling curves of VGO4, VGO4 + 100 ppm AMAC, and VGO4 + 100 ppm EMAC were first obtained under non-isothermal conditions, and then, the heat capacity signal was subtracted from the DSC curves by using a specific heat measurement method to get the latent heat of crystallization for the three samples. Based on this, the non-isothermal crystallization kinetics were investigated.

The non-isothermal crystallization DSC curves of the paraffin crystals of VGO4 with and without additives at different cooling rates are shown in Figure 7. The basic parameters, onset temperature (T_0), terminal temperature (T_∞), and peak temperature (T_P), were obtained from the DSC curves. According to Figure 7, all the samples only had one exothermic peak at different cooling rates, indicating that the change of the cooling rate and the addition of the comb polymer does not change the crystallization properties. As the cooling rate (ϕ) increased, the crystallization exothermic peak intensity gradually increased, and the peak temperature maximum moved towards a low temperature. This is because the supersaturation state of paraffin in the system was formed rapidly when the cooling rate was high, resulting in the formation of a large number of crystal nuclei at the initial crystallization stage, and thus, the paraffin crystals were homogeneously distributed in the whole system. Subsequently, the heterogeneity of the crystallization process predominated, and the crystal morphology became imperfect.

The non-isothermal crystallization parameters of the paraffin in VGO4 with and without the comb-type copolymer are shown in Tables 8–10, respectively. Comparing the data in Table 8 with that in Tables 9 and 10, the T_0 values moved in the high-temperature direction, and the wax precipitation point increased when the two kinds of comb-type copolymers were added, respectively. At this time, the paraffin crystals were more likely to be separated from VGO4, because these comb-type copolymers had a higher solidification point, and they crystallized first at a temperature higher than the paraffin precipitation point of VGO4. This confirmed that the comb-type copolymers played a key role in heterogeneous nucleation in the process of paraffin crystal precipitation. In addition, at the same cooling rate, the ($T_0 - T_\infty$) value of VGO4 with the comb-type copolymer decreased, and the crystallization time of paraffin was shorter.

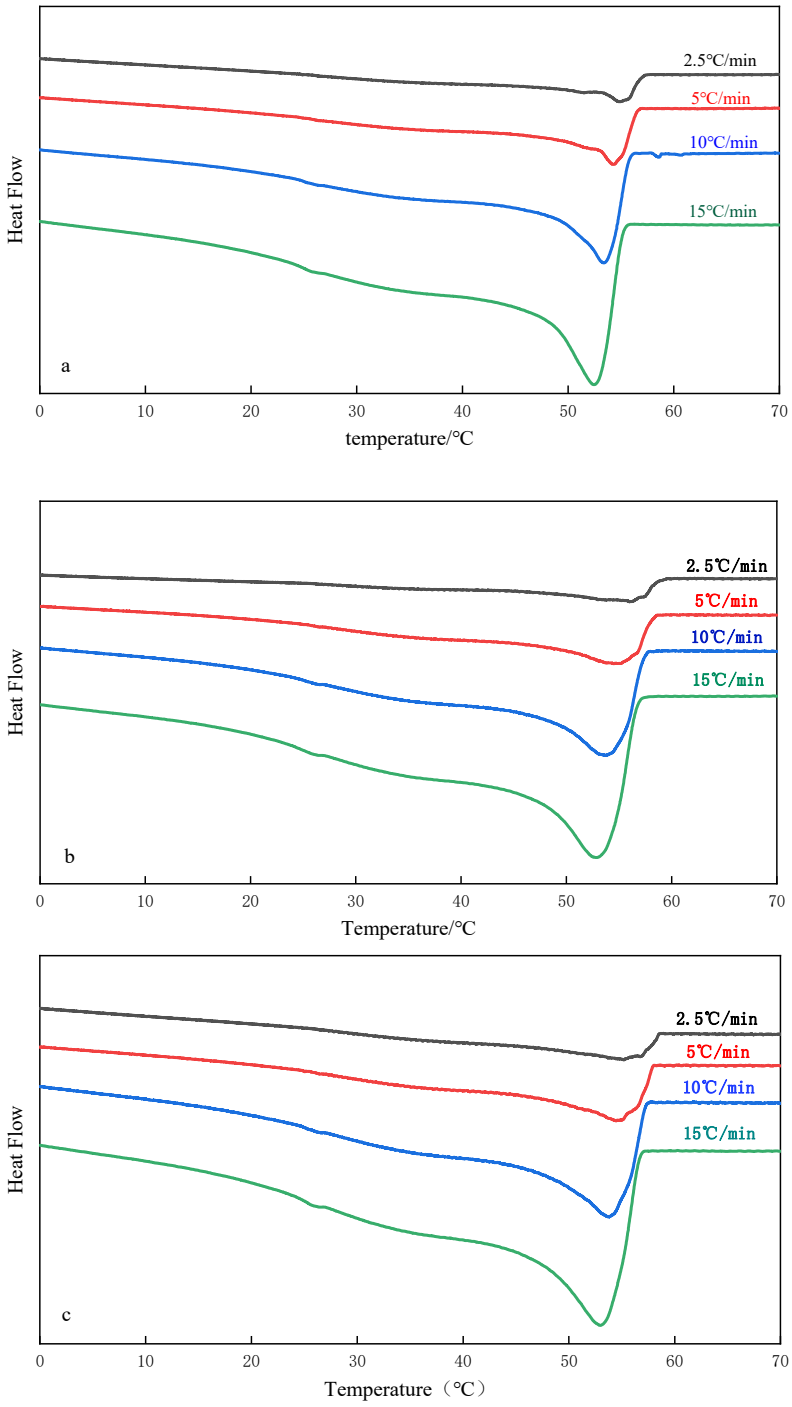

Figure 7. Non-isothermal crystallization DSC curves of different samples at various cooling rates: (**a**) VGO4, (**b**) VGO4 + 100 ppm AMAC, and (**c**) VGO4 + 100 ppm EMAC.

Table 8. The non-isothermal crystallization parameters of VGO4.

ϕ/(°C·min^{-1})	T_0/°C	T_∞/°C	T_P/°C	$(T_0 - T_\infty)$/°C
2.5	57.95	22.17	54.93	35.78
5	57.08	20.96	54.36	36.12
10	56.83	20.69	53.49	36.14
15	56.18	19.27	52.66	36.91

Table 9. The non-isothermal crystallization parameters in the presence of 100 ppm AMAC.

ϕ/(°C·min^{-1})	T_0/°C	T_∞/°C	T_P/°C	$(T_0 - T_\infty)$/°C
2.5	59.72	25.18	56.23	34.54
5	58.85	24.26	55.21	34.59
10	58.06	22.71	54.36	35.35
15	57.85	22.29	53.34	35.56

Table 10. The non-isothermal crystallization parameters in the presence of 100 ppm EMAC.

ϕ/(°C·min^{-1})	T_0/°C	T_∞/°C	T_P/°C	$(T_0 - T_\infty)$/°C
2.5	58.73	23.92	55.20	34.81
5	58.18	23.25	55.01	34.93
10	57.73	22.49	53.87	35.24
15	57.20	21.40	53.23	35.80

3.6. Crystallization Kinetics

As far as the paraffin in VGO4 is concerned, its crystal structure and size are mainly determined by the two stages of the crystallization process: crystal nucleus formation and crystal nucleus growth. Therefore, studying the role of comb-type copolymers in the two stages is of great significance for improving the production efficiency of the MEK–toluene unit. In this study, the entire crystallization process of paraffin in VGO4 with AMAC or EMAC was investigated by using the equation proposed by Mo to determine the effects of AMAC and EMAC on the paraffin crystallization process in VGO4.

Based on the Avrami equation and the Ozawa equation, Mo derives the following non-isothermal crystallization equation by considering the relationship between the relative crystallinity, cooling rate (ϕ), and crystallization time (t) [30]:

$$\lg\phi = \ln F(T) - \alpha \lg t \tag{1}$$

where $F(T)$ is the cooling rate required to reach a certain relative crystallinity in a unit of time, and parameter α is the ratio of the Avrami index to the Ozawa index. t is the time of the wax crystal reaching a certain crystallinity, which was calculated as follows:

$$t = \frac{|T - T_0|}{\phi} \tag{2}$$

The calculation of the relative crystallinity $X(t)$ at any temperature is according to Formula (3):

$$X_t = \frac{\int_{T_0}^{T} \left(\frac{dH}{dT}\right) dT}{\int_{T_0}^{T_\infty} \left(\frac{dH}{dT}\right) dT} \tag{3}$$

where $\frac{dH}{dT}$ refers to the heat flow rate at a certain temperature, T_0 is the onset temperature of crystallization, and T_∞ is the terminal temperature of the crystallization. T_0, T_∞, and T are from −20 °C to 80 °C.

The relationship between the relative crystallinity and temperature of the three samples at different cooling rates was plotted in Figure 8. For all three samples, the crystallization rate was much greater in the early stage of crystallization. As the relative crystallinity was raised from 0.8 to 1.0, the crystals collided with and squeezed each other due to the increase of crystallinity, the crystallization rate decreased, and the curve tended to be flat. In addition, to achieve the same relative crystallinity at the same cooling rate, it takes a wider temperature range for the sample without comb-type copolymer additives.

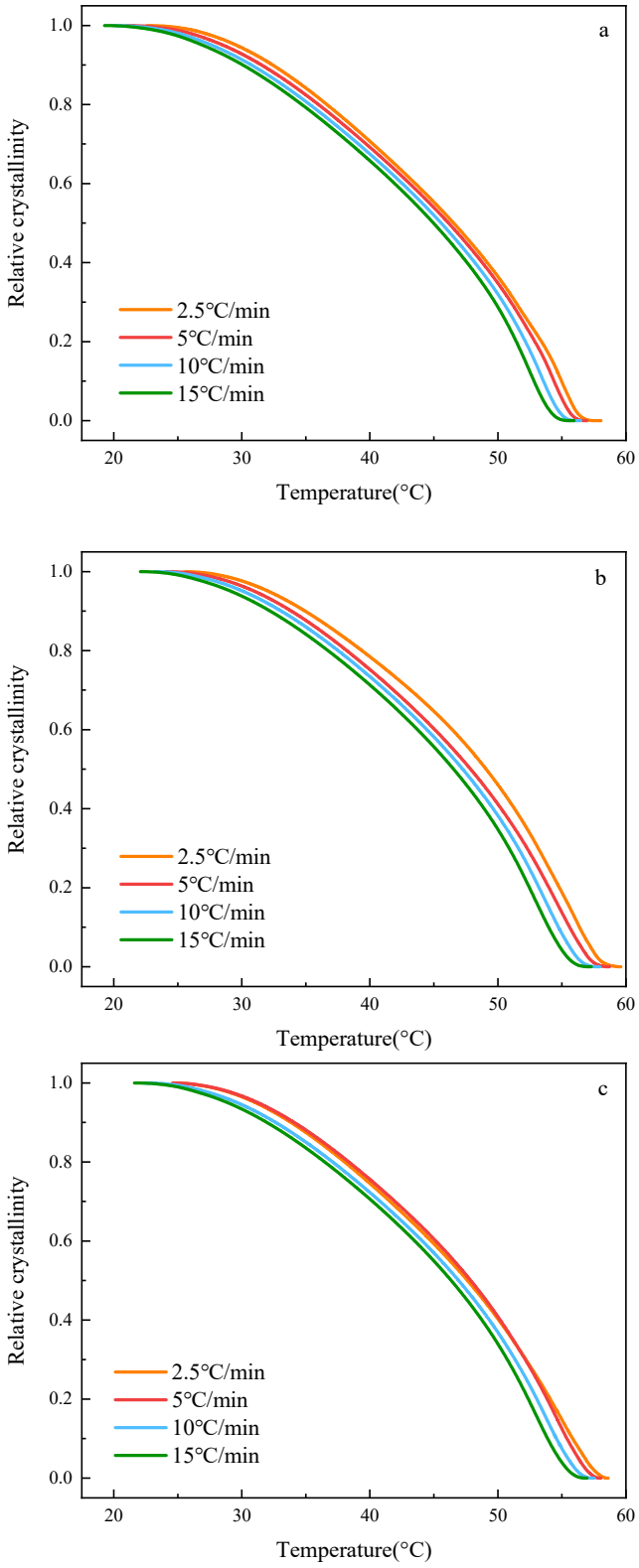

Figure 8. Relationship between the relative crystallinity and temperature at different cooling rate: (**a**) VGO4, (**b**) VGO4 + 100 ppm AMAC, and (**c**) VGO4 + 100 ppm EMAC.

According to Formula (1), the plots of lnϕ as a function of ln$t$ are shown in Figure 9. The plots of the three samples are almost parallel straight lines, indicating that these two parameters had a good linear relationship. This work confirms that the equation proposed by Mo is suitable for studying the non-isothermal crystallization process of paraffin in

VGO4. The intercept $F(t)$ and the slope α were obtained from Figure 9, where $F(t)$ can reflect the rate of the crystallization, and the larger the $F(t)$ is, the smaller the crystallization rate. The parameters reported in Table 11 showed that, when the cooling rate was the same, the crystallization rate of paraffin in VGO4 with comb-type copolymers was higher than that in VGO4, indicating that the AMAC and EMAC comb-type copolymers promoted the crystallization process and increased the crystallization rate of paraffin, which led to the crystals more aggregated and the crystallite size big, and therefore, relatively complete morphologies of the crystals were observed. These modifications increased the filtration speed and enhanced the production efficiency of the MEK–toluene unit.

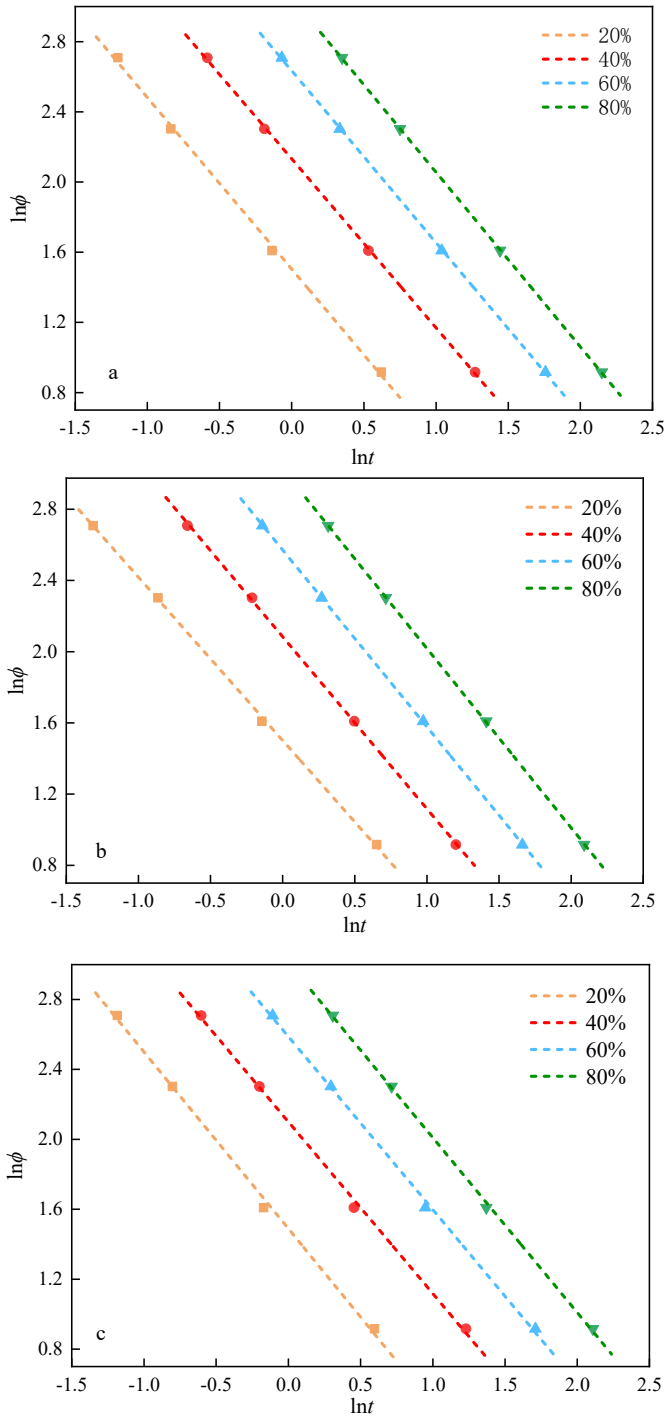

Figure 9. The lnϕ as a function of ln$t$: (**a**) VGO4, (**b**) VGO4 + 100 ppm AMAC, and (**c**) VGO4 + 100 ppm EMAC.

Table 11. Values of the intercept ($F(t)$) and slope (α) are obtained from Figure 9.

Relative Crystallinity/%	VGO4		VGO4 + 100 ppm AMAC		VGO4 + 100 ppm EMAC	
	$F(t)$	α	$F(t)$	α	$F(t)$	α
20	4.51	0.98	4.44	1.00	4.32	1.01
40	8.50	0.96	7.82	1.00	8.01	0.98
60	14.01	0.98	12.54	1.01	12.99	0.99
80	21.27	0.99	20.51	1.01	19.81	1.00

4. Conclusions

Two comb-type copolymers were synthesized and successfully applied in the MEK–toluene dewaxing process. Various factors such as the ketone–aromatics ratio, solvent ratio, and filtration temperature were investigated in the process with three-stage dilution and two-stage deoiling. The results showed that the yield of DWO increased from 67.21% to 70.87% by adding 100 ppm AMAC and 69.90% by adding 100 ppm EMAC under the conditions of ketone–aromatics ratio of 6:0, solvent ratio of 5:1, and dewaxing temperature at −12°C. On the basis of the analysis of the non-isothermal crystallization kinetics and PLM observations, it could be concluded that the addition of AMAC and EMAC could accelerate the crystallization rate of paraffin in MEK–toluene dewaxing by forming three-dimensional snow flower-like nanocrystals or rods with longer sizes and more perfect crystal morphology, favoring the enhancement of the filtration rate and the production efficiency of the MEK–toluene dewaxing process.

Author Contributions: Data curation, Y.X. and Z.W.; Investigation, X.N.; Methodology, Y.X., H.L. and L.C.; Writing—original draft, Y.X.; Writing—review & editing, Y.X., Y.S., J.W., X.Z. and L.C. All authors have read and agreed to the published version of the manuscript.

Funding: This research was financially supported by the projects of the Instituto Politécnico Nacional (Grants No. SIP-20210451 and 20220117).

Data Availability Statement: Not applicable.

Conflicts of Interest: The authors declare no conflict of interest.

Abbreviations

DWO	Dewaxed oil
WAX	Deoiled wax
FO	Foots oil
MEK	Methyl ethyl ketone
VGO4	Forth cut of vacuum gas oil
BPO	Benzoyl peroxide
DSC	Differential scanning calorimetry
PLM	Polarizing light microscope
AMAC	Maleic anhydride-α-octadecene copolymer with aniline
EMAC	Maleic anhydride-α-octadecene copolymer with phenethylamine
Symbols	
T_0	Crystallization onset temperature
T_P	Crystallization peak temperature
T_∞	Crystallization termination temperature
$T_0 - T_\infty$	Temperature range required for crystallization
Φ	Cooling rate
T	Temperature
$F(t)$	Cooling rate required to reach a certain relative crystallinity in unit time
α	The ratio of Avrami index to Ozawa index

References

1. Giorgio, S.; Kern, R. Filtrability, crystal morphology and texture; Paraffins and dewaxing aids. *J. Cryst. Growth* **1983**, *62*, 360–374. [CrossRef]
2. Alain, H.; Bernard, P. How does a Cloud Point diesel fuel additive work? *J. Colloid Interface Sci.* **1992**, *1992*, 153.
3. Ashbaugh, H.S.; Guo, X.H.; Schwahn, D.; Prud'homme, R.K.; Richter, D.; Fetters, L.J. Interaction of paraffin wax gels with ethylene/vinyl acetate co-polymers. *Energy Fuels* **2005**, *19*, 138–144. [CrossRef]
4. Castro, L.V.; Vazquez, F. Copolymers as Flow Improvers for Mexican Crude Oils. *Energy Fuels* **2008**, *22*, 4006–4011. [CrossRef]
5. Guo, X.H.; Pethica, B.A.; Huang, J.S.; Prud'homme, R.K.; Adamson, D.H.; Fetters, L.J. Crystallization of mixed paraffin from model waxy oils and the influence of micro-crystalline poly(ethylene-butene) random copolymers. *Energy Fuels* **2004**, *18*, 930–937. [CrossRef]
6. Li, L.; Guo, X.H.; Adamson, D.H.; Pethica, B.A.; Huang, J.S.; Prud'homme, R.K. Flow Improvement of Waxy Oils by Modulating Long-Chain Paraffin Crystallization with Comb Polymers: An Observation by X-ray Diffraction. *Ind. Eng. Chem. Res.* **2011**, *50*, 316–321. [CrossRef]
7. Soni, H.P.; Agrawal, K.S.; Nagard, A.; Bharambe, D.P. Designing maleic anhydride-alpha-olifin copolymeric combs as wax crystal growth nucleators. *Fuel Processing Technol.* **2010**, *91*, 997–1004. [CrossRef]
8. Soni, H.P.; Bharambe, D.P. Performance-Based Designing Of Wax Crystal Growth Inhibitors. *Energy Fuels* **2008**, *22*, 3930–3938. [CrossRef]
9. ESSO RES & ENG CO(ESSO-C). Dewaxing Mineral Oil Using Dewaxing Aids Optionally. U.S. Patent Application No. US3458430-A; GB Patent Application No. GB1151385-A; U.S. Patent Application No. CA886554-A, 5 January 1968.
10. SANYO CHEM IND LTD(SANN-C). Dewaxing Aid Prepn.—by Reacting Naphthalene and Chlorinated Paraffin in Presence of Friedel-Crafts Reagent. International Patent Application No. JP1240596-A, 6 January 1989.
11. EXXON RES & ENG CO(ESSO-C), IMPERIAL OIL LTD(IMOI-C). Hydrocarbon Oil solVent Dewaxing Aid—Comprising Lithium Iso: Stearate and a Polymer of an Aliphatic Alcohol (Meth) Acrylic Ester. International Patent Application No. GB2048922-A; JP55149387-A; FR2455627-A; GB2048922-B; CA1147689-A; JP89042994-B; IT1209215-B, 4 January 1980.
12. Monjiyama, S.; Kawamoto, H.; Oda, K. Aid for Solvent Dewaxing, Comprises Ethylene-Alpha-olefin Copolymer Containing Ethylene and Alpha-Olefin in Preset Molar Ratio, and Having Preset Weight Average Molecular Weight. International Patent Application No. WO2021145309-A1, 8 January 2022.
13. Yang, K.; Yang, W.; Ding, L. Solvent Dewaxing and De-Oiling Process Comprises Use of Filter Aid. International Patent Application No. CN1344783-A; CN1152122-C, 4 January 2004.
14. Guan, C.; Wang, Y.; Yang, W.; Ding, L. Effect of dewaxing additives on wax crystallization in solvent dewaxing process. *Pet. Process. Petrochem.* **2009**, *40*, 8–12.
15. Wang, H.; Deng, Y.; Huang, C.; Zhao, Y. *Application of Dewaxing Assistant LSDA-1 in Solvent Dewaxing of Xinjiang Vacuum Distillate*; China Society for Petrochemical Information: Beijing, China, 2001; pp. 846–850.
16. Ren, P.; Sheng, K. Application of filter aid SM-40 in microcrystalline wax production in MEK-toluene plant. *Pet. Natural Gas Chem. Ind.* **2002**, *33*, 59–61.
17. Hennessy, A.; Neville, A.; Roberts, K.J. In-situ SAXS/WAXS and turbidity studies of the structure and composition of multihomologous n-alkane waxes crystallized in the absence and presence of flow improving additive species. *Cryst. Growth Des.* **2004**, *4*, 1069–1078. [CrossRef]
18. Wu, C.J.; Zhang, J.L.; Li, W.; Wu, N. Molecular dynamics simulation guiding the improvement of EVA-type pour point depressant. *Fuel* **2005**, *84*, 2039–2047. [CrossRef]
19. Zhang, J.L.; Zhang, M.; Wan, J.J.; Li, W. Theoretical study of the prohibited mechanism for ethylene/vinyl acetate co-polymers to the wax crystal growth. *J. Phys. Chem. B* **2008**, *112*, 36–43. [CrossRef]
20. Li, X.; Lu, S.; Niu, M.; Cheng, R.; Gong, Y.; Xu, J. Asphaltene Inhibition And Flow Improvement Of Crude Oil With A High Content Of Asphaltene And Wax By Polymers Bearing Ultra-Long Side Chain. *Energies* **2021**, *14*, 8243. [CrossRef]
21. Cheng, R.; Zou, R.; He, L.; Liu, L.; Cao, C.; Li, X.; Guo, X.; Xu, J. Effect Of Aromatic Pendants In A Maleic Anhydride-Co-Octadecene Polymer On The Precipitation Of Asphaltenes Extracted From Heavy Crude Oil. *Energy Fuels* **2021**, *35*, 10562–10574. [CrossRef]
22. Gaylord, N.G.; Mehta, R.; Mohan, D.R.; Kumar, V. Maleation of linear low-density polyethylene by reactive processing. *J. Appl. Polym. Sci.* **1992**, *44*, 1941–1949. [CrossRef]
23. He, C.Z.; Ding, Y.F.; Chen, J.; Wang, F.; Gao, C.; Zhang, S.; Yang, M. Influence of the nano-hybrid pour point depressant on flow properties of waxy crude oil. *Fuel* **2016**, *167*, 40–48. [CrossRef]
24. Li, N.; Mao, G.; Wu, W.; Liu, Y. Effect evaluation of ethylene vinyl acetate/nano-montmorillonite pour-point depressant on improving the flow properties of model oil. *Colloids Surf. A Physicochem. Eng. Asp.* **2018**, *555*, 296–303. [CrossRef]
25. Wang, F.; Zhang, D.M.; Ding, Y.F.; Zhang, L.X.; Yang, M.S.; Jiang, B.L.; Zhang, S.M.; Ai, M.; Liu, G.; Zhi, S.; et al. The effect of nanohybrid materials on the pour-point and viscosity depressing of waxy crude oil. *Chin. Sci. Bull.* **2011**, *56*, 14–17. [CrossRef]
26. Xu, J.; Xing, S.L.; Qian, H.Q.; Chen, S.; Wei, X.M.; Zhang, R.; Li, L.; Guo, X.H. Effect of polar/nonpolar groups in comb-type copolymers on cold flowability and paraffin crystallization of waxy oils. *Fuel* **2013**, *103*, 600–605. [CrossRef]

27. Zhang, D.M.; Zhang, L.X.; Huo, L.F.; Zhi, S.J.; Ouyang, X.; Xu, B.; Xiong, H.; Jiang, B.L.; Li, J.T.; Wang, S. Application of nano-material based hybrid pour-point depressant for long-distance waxy crude pipeline. In Proceedings of the 9th International Pipeline Conference (Ipc 2012), Calgary, Canada, 24–28 September 2012; p. 2013.
28. Wang, T.S.; Xu, J.; Wang, M.L.; Wei, X.M.; Shen, M.X.; Huang, J.; Zhang, R.; Li, L.; Guo, X.H. Synthesis of comb-type copolymers with various pendants and their effect on the complex rheological behaviors of waxy oils. *J. Appl. Polym. Sci.* **2015**, *132*, 41660. [CrossRef]
29. Zhao, H.Q.; Xu, J.; Li, T.; Wang, T.S.; Wei, X.M.; Wang, J.; Xu, Y.S.; Li, L.; Guo, X.H. Effect Of Heteroaromatic Pendants In Comb Copolymers On Paraffin Crystallization And Cold Flow Ability Of Crude Oil. *Energy Fuels* **2016**, *30*, 5398–5403. [CrossRef]
30. Mo, Z.S. A method for the non-isothermal crystallization kinetics of polymers. *Acta Polym. Sin.* **2008**, *7*, 656–661. [CrossRef]